Comparison of transformation behavior of the peritectic steels with different carbon content and its correlation to the slab quality during solidification

Ahmad Zamanian[1], Nam Hoon Goo[1*], Tahereh Zargar[1,2], Fazlollah Sadeghi[1,3], Soo Yeon Lee[1], Yoon Uk Heo[1], Jae Sang Lee[1], Dae Geun Hong[1], Jong Hyun Kim[4], Ho Jae Kwak[4], Seong Gyoon Kim[5], Nam Cheol Hee[6], Chang Hee Yim[1*]

Abstract

In order to investigate the phase transformation behaviour of peritectic steels, we devise an integrated facility for X-ray transmission imaging combined with Laue diffraction analysis and precise temperature control. This integrated facility can measure the temperature at which the delta phase transforms into the gamma phase during solidification with continuous cooling. The investigation of four alloys with different carbon content reveals the dependence of carbon content on the minimum undercooling required for gamma phase formation. As carbon content increases, the amount of undercooling for the peritectic transformation decreases, and the gamma phase onset temperature necessarily increases. X-ray transmission images, which present the growing dendrites and moving delta-to-gamma interface, confirm that the peritectic reaction is likely to occur with high carbon content, leading to the gamma phase formation before the end of solidification.

On the contrary, the low carbon content suppresses the gamma phase formation, and the solid delta and liquid phase exist under equilibrium peritectic temperature. Once after the gamma phase nucleation, the phase change occurs rapidly with increasing undercooling. The delay in gamma phase formation results in massive phase transition and rapid change of interface velocity with a slight variation of undercooling. The fast kinetic of solid phase transformation is associated with a corresponding increase of internal stress, leading to the degradation of slab quality.

[1] Graduate Institute of Ferrous and energy materials Technology, Pohang University of Science and Technology, Pohang 37673, Republic of Korea
[2] Faculty of Natural, Mathematical & Engineering Sciences, King's College London, Strand, London WC2R 2LS, United Kingdom
[3] Brunel Center for Advanced Solidification (BCAST), Brunel University, Middlesex, London, UB8 3PH, United Kingdom
[4] Pohang Accelerator Laboratory, Pohang, 37673, South Korea
[5] Kookmin University, Seoul, 02707, South Korea
[6] Technical Research Laboratory, POSCO, Gwangyang 57812, South Korea

Keyword: Peritectic steel, In situ X-ray, Carbon content, massive phase transition

1. Introduction

The low carbon steels having the carbon content in the peritectic region, are used for various structural applications. The sufficient carbon content provides the efficient way to increase strength level over 500MPa, and proper toughness even in low temperature because of suppression of brittle carbide phases. [1], [2], [3]

However, the phase transformation of the steels is not simple in particular at high temperatures of solidification. The Fe-C equilibrium diagram presents liquid and two allotriomorphic solid phases of delta and gamma. With the carbon content less than 0.01wt%, the delta and gamma phase transition are completely separated, but in the carbon range of peritectic, there is a region of three phases, which is called the peritectic reaction. [4] [5] [6]

Not only in the steel alloys, but also in other alloy systems, such as Fe-Ni, Nd-Fe-B, the peritectic region is presented in the equilibrium phase diagram. [7] In particular the peritectic reaction of steel is problematic because of the high nucleation barrier of the gamma phase. The nucleation barrier retards the gamma phase formation in the equilibrium peritectic region and the solidification ends even with the delta phase solely. After a proper undercooling endows nucleation driving force for the gamma phase, the remaining delta phase transforms to the gamma. This delta gamma transformation is still ambiguous in the kinetic analysis. [8] [9] [10] [11]

Some people report the transition kinetics is abrupt and diffusionless manner, so called the massive transformation. Others proclaim that it is a diffusional process but very fast, called massive like transformation [12]. It is clear that when the condition of cooling is close to the equilibrium the delta to gamma transition takes place after the gamma phase is nucleated at the boundary between liquid and delta phase. With the deviation from the equilibrium condition, that is, increase of undercooling, the delta to gamma transition becomes faster and diffusionless. [10] [13] [14]

The influence of carbon is another important aspect of the peritectic transformation. It is well known that when it comes to the peritectic composition of carbon, at the lower limit of carbon, c.a. 0.1wt% the gamma phase tends to be suppressed and the delta to gamma transition proceeds without liquid phase and it is also very fast. On the contrary at the higher limit of carbon, c.a. 0.5wt%, the gamma phase nucleation becomes easier and the delta to gamma transition closely followed by the peritectic reaction (Liquid + delta → gamma). [15] [16] [17]

There is still arguing whether the gamma phase formation after the peritectic reaction is the diffusion engaged or not, but the observed reports have been consistently shown that the kinetic transformation with peritectic reaction becomes slower than without peritectic reaction [18], [19] [20] [21] [22]

Considering the ratio of the liquid phase to the delta phase, which is the initial solidification phase, determined by the lever rule in the equilibrium diagram, and considering that the carbon required for nucleation of the gamma phase is supplied by the liquid phase, it can be qualitatively judged that the nucleation of the gamma phase is easier in the region with higher carbon than in the region with lower carbon. However, this is only a qualitative description, and there are still very few reports that quantitatively describe or observe the transition from delta phase to gamma phase. For an efficient and valuable steel alloy design the peritectic range of carbon content is inevitable, and many steel works have been struggling with the issues arising from slabs with peritection range of compositions. In particular the hypo perictectic range, i.e. the carbon content below the peritectic point, difficulties of slab casting involved in the fast peritectic reaction increases and most problematic carbon composition is on the lower limit of the peritectic range, c.a. 0.1wt%. The volume changes involved in the delta to gamma transition are high enough to create surface undulation or cracks at the slab surface in the vicinity of the solid shell. In current most slab manufacturing will use a continuous casting process, and in continuous casting, the rate of solidification and subcooling on the mold surface

Although the mechanism of the reaction has been elucidated by previous studies, kinetic observations of the peritectic reaction at different carbon contents in real steel materials have not been reported to date. In this study, we utilize real-time X-ray observation equipment to observe the stages of peritectic reaction and peritectic transformation from the time of solidification and calculate the rate of phase change. From this, we will analyze the sensitivity of the phase transformation to changes in supercooling and determine how the sensitivity to supercooling changes with changes in carbon content. We will also examine how the results of the analysis correlate with the extent of defects observed in slabs that simulate the actual continuous casting process.

2. Experimental methods

In-situ observations were conducted at Beamline 9D WX at the Pohang Light Source-II, Korea, utilizing a synchrotron white beam X-ray source. This high-intensity X-ray beam, capable of penetrating thick carbon steel samples, was employed to facilitate detailed in-situ imaging during the unidirectional solidification process. A B-type thermocouple was placed on the sample within the furnace to continuously monitor and record the sample temperature during both the heating and cooling phases of the experiment. This setup allowed for precise thermal profiling of the sample, providing essential data to analyze the solidification dynamics under controlled conditions.

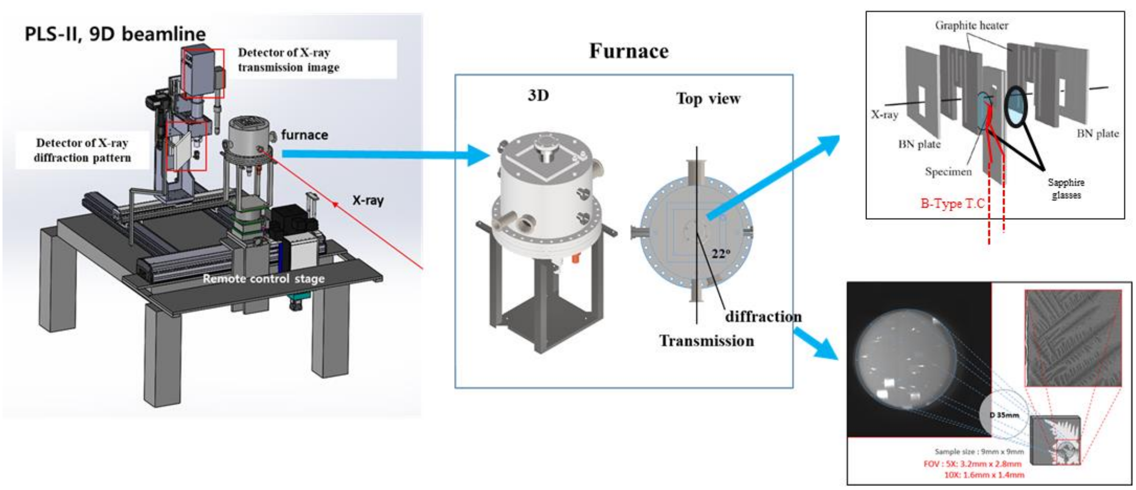

Fig. 1. Schematic illustration of the experimental setup

The 3D schematic structure of the vacuum chamber, along with the top view of the transmitted and diffracted beams and the observation area during the experiment, is displayed in Figures 1. Comprehensive descriptions of the setup, including the characteristics of the synchrotron X-ray source, and detailed imaging of the solidification process were provided in our previous studies [23, 24]. A summary of details regarding the X-ray source and the imaging of the solidification process are presented in Table 1.

Table 1. Processing parameters for in-situ observation

parameter		Value
Detector	Transmitted camera (Pixel size)	PCO edge 5.5 (6.5 µm/pixel)
	Diffracted detector (Pixel size)	VIVIX-D 0606C (119 µm/pixel)
Sample Dimension		10 mm × 10 mm × 0.5 mm
Observation area size		3.33 mm ×2.81 mm
Spatial resolution (Pixel size)		1.3 µm (With 5X magnification objective lens)
Acquisition frame rate	Transmission	5 fps
	Diffraction	10 fps
	Temperature	5 fps
Cooling rate		5 to 500 °C/min

Four industrial peritectic carbon steel specimens (Table 2) were examined to observe the effect of varying carbon equivalent contents on the δ to γ transformation behavior. The alloys were cut, polished, and cleaned to achieve final dimensions of 10 mm × 10 mm × 500 µm (width × length × thickness). Alloying elements, in addition to carbon, alter the effective carbon content and shift the peritectic range [25]. Various models for calculating the carbon equivalent (CP) of steel alloys have been proposed, and the model developed by Normanton [26] was utilized in this study.

$$C_P = [C] + 0.01[Mn] + 0.009[Si] + 0.02[Ni] + 0.003[Cr] - 0.007[Mo] + 0.009[V] + 0.008[P] + 0.147[S] + 0.5[N] + 0.007[Cu] + 0.007[Ti] + 0.05[Al] + 0.04[Nb] \quad \text{(eq. 1)}$$

Table 2. Nominal chemical compositions of the steels employed in this study and carbon equivalent calculation

Steel Code	**Fe**	**C%**	**Mn%**	**Si%**	**Other elements (P, S, Ni, Cu, Ti, Nb)**	**%Cp equivalent**
Steel A	Bal.	0.06	1.44	0.26	0.62	0.087
Steel B	Bal.	0.14	0.55	0.6	0.3	0.156

Steel C	Bal.	0.19	0.5	0.25	0.0	0.197
Steel D	Bal.	0.44	0.6	0.21	0.032	0.482

Equilibrium calculations were carried out using Thermo-Calc (database: TCFE13) to map these peritectic steel grades onto the phase diagram, as depicted in Figure 2. Steel A and B fall within the hypo-peritectic region, whereas Steel C and D are positioned in the hyper-peritectic region.

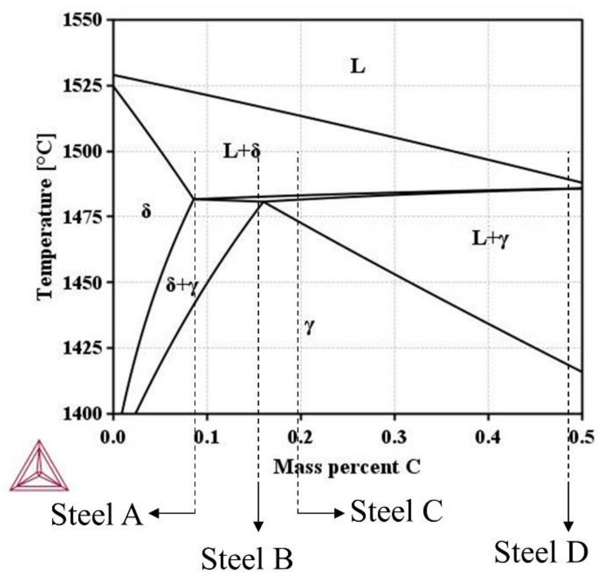

Fig. 2. Equilibrium pseudo-binary phase diagram, composition indicator lines

3. Results

To thoroughly investigate the δ to γ transformation in four peritectic steel grades, we conducted numerous experiments at varying cooling rates from 5°C/min to 500°C/min. Initially, we present typical observations of sample temperature profiles, images, and Laue patterns as representative cases. These preliminary observations set the stage for a comprehensive explanation of the results that follow.

3.1. Typical sample temperature profile during solidification of peritectic steel grades

As described in our previous study [24], the accuracy of the temperature measurements was determined to be within ±5 °C. In the measured time-temperature profile (Figure 3), the temperature curves display distinct features associated with phase changes. Initially, the temperature was raised above the equilibrium melting point to ensure the complete melting of the alloy. Three different profiles were recorded during the cooling stages of the experiment, as shown in Figure 3. In Figure 3a, two peaks (P1 and P2) are present in the temperature profile. As the temperature falls far below the liquidus point, a sudden rise, known as recalescence, occurs (P1). It is noteworthy that when the undercooling for solidification is approximately less than 15°C, no peak (P1 point) is observed during dendrite nucleation (Figures 3b and 3c). Further cooling can lead to another noticeable temperature increase, attributed to the transition from the δ to γ phase, observed in Figures 3a and 3b (P2). However, in Figure 3c, no peak is observed during this transformation. The mode of transformation (slow or fast) and the amount of undercooling from equilibrium affect the presence and magnitude of peaks in the temperature profile.

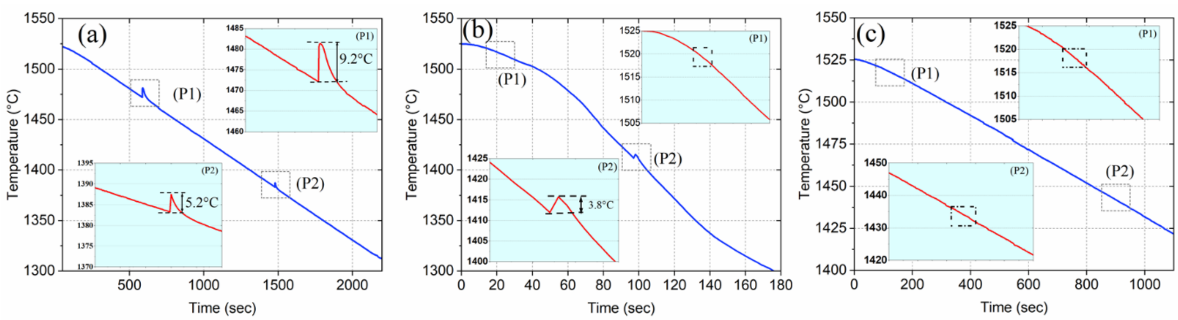

Fig. 3. Typical temperature profile of specimen during cooling; temperature profile when both recalescence and fast δ to γ transition occurred- Steel A, Cooling rate: 6.5ºC/min (a), only fast δ to γ transition- Steel A, Cooling rate: 110ºC/min (b), and slow δ to γ transition- Steel A, Cooling rate: 6ºC/min (c).

3.2. Typical transmitted images and Laue pattern during phase transformation of peritectic steel grades

In these four peritectic steel grades, two different modes of the δ to γ transformation were observed, each represented by a case study in this section. The first mode, illustrated in Figure 4, is characterized by a small degree of undercooling for the δ to γ transformation. According to Table 3, the equilibrium temperature for the initiation of this transformation for this case study is 1488.6°C. However, during the experiment, the transformation began at 18.6°C below this temperature. In this scenario, as depicted in Figure 4, the average interface velocity of the δ/γ phases was observed to be as slow as 0.6 mm/sec during the transformation. The Laue pattern for this case clearly indicates that, at the time of the transition, the δ-phase pattern (red color) begins to fade, while the γ-phase pattern (blue color) emerges.

Table 3. Details for the case study on **small** undercooling in the δ to γ transformation

Steel Code	**Cooling rate (°C/min)**	**Equilibrium (δ →γ) temperature (°C)**	**Measurement (δ →γ) temperature (°C)**	**Undercooling for initiation of transformation (°C)**	$t_{0.5}$	n
Steel C	110	1488.6	1470	18.6	0.94	0.85

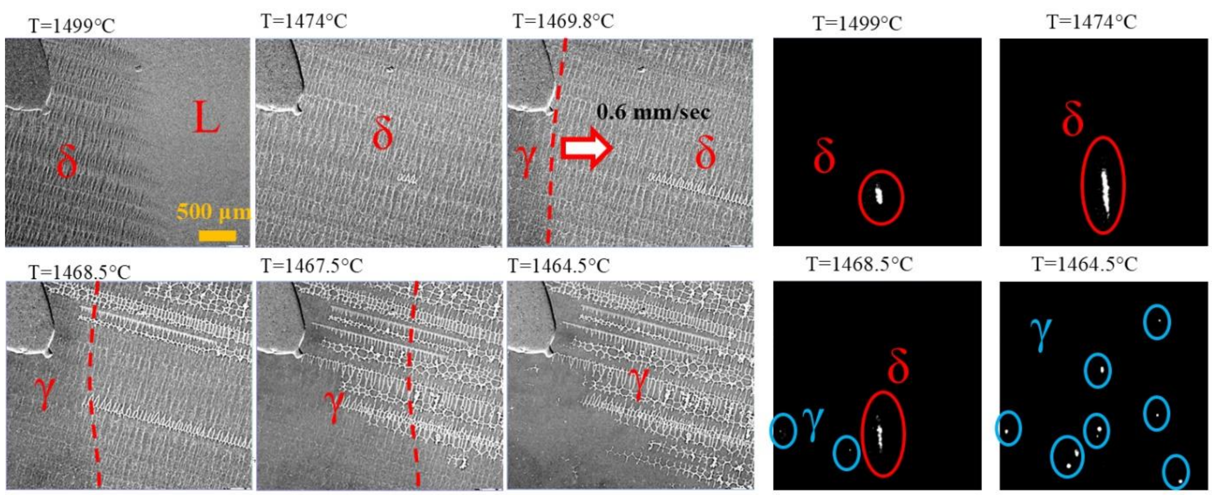

Fig. 4. Transmission images, Laue pattern and temperature value during transformation for small undercooling - Steel C, Cooling rate: 110ºC/min

To analyze the kinetic transformation in this case study, we employed the method outlined in our previous study [24]. This approach involves counting the diffraction intensity and correlating it with the volume fraction of the δ phase. The data was then fitted to an Arrhenius-type model for phase transformation (Equation 2).

$$X = 1 - \ exp\left[-log2 \cdot \left(\frac{t}{t_{0.5}}\right)^{n}\right] \text{ (eq. 2)}$$

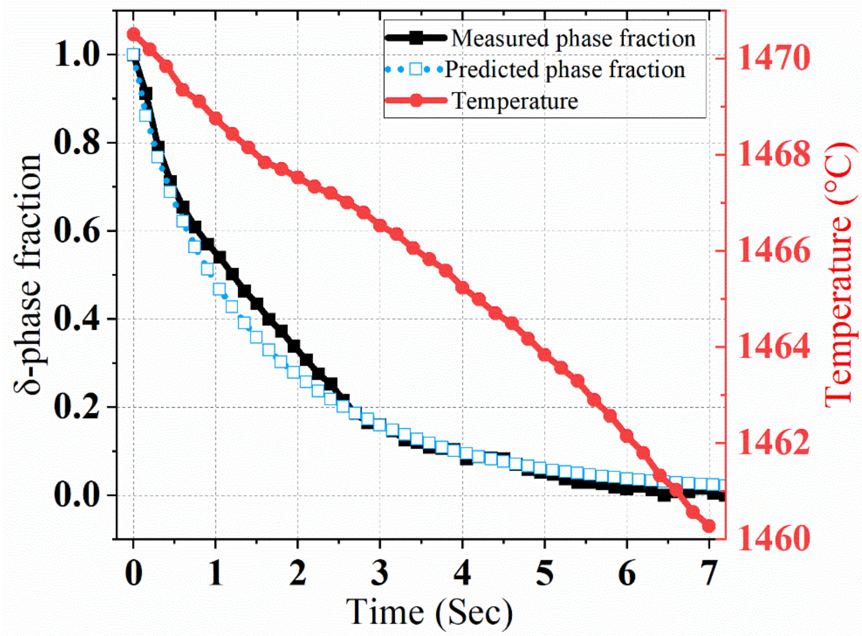

Fig. 5. The temperature profile and phase fraction of the delta phase (measured and predicted) in small undercooling case study- Steel C, Cooling rate: 110ºC/min.

The parameters $t_{0.5}$ and n, which describe the transformation kinetics, were calculated and are presented in Table 3. Figure 5 illustrates the temperature profile alongside the measured and predicted δ phase volume fractions. As shown in the temperature graph, the slope changes during the transformation due to the release of latent heat. However, because this transition occurs slowly, the released heat spreads into the surrounding area, preventing the formation of a noticeable peak in the temperature graph.

Table 4. Details for the case study on **big** undercooling in the δ to γ transformation

Steel Code	**Cooling rate (°C/min)**	**Equilibrium (δ →γ) temperature (°C)**	**Measurement (δ →γ) temperature (°C)**	**Undercooling for initiation of transformation (°C)**	$t_{0.5}$	n
Steel C	30	1488.6	1410.5	78.6	0.096	2.1

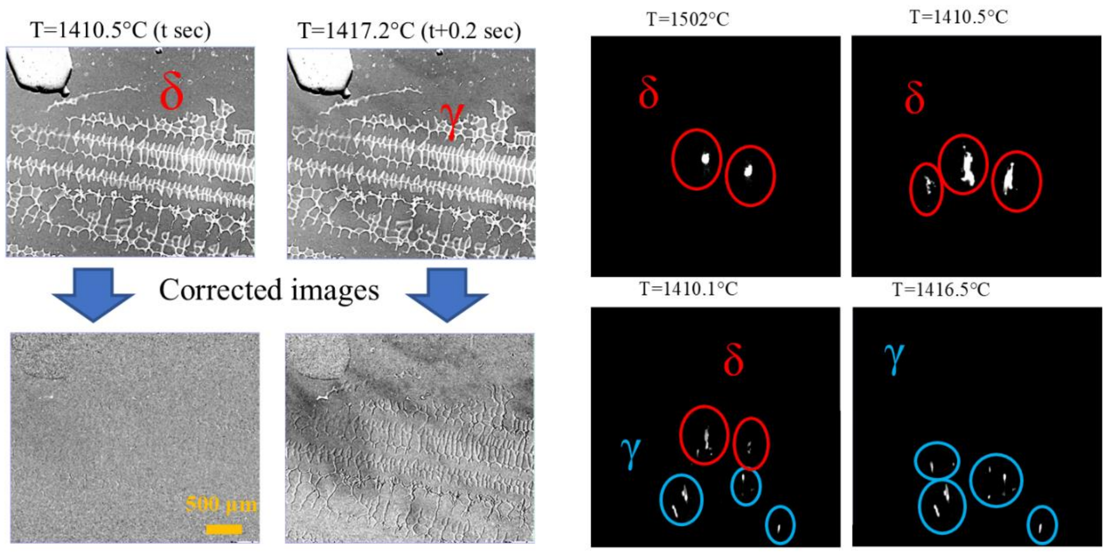

Fig. 6. Transmission images, Laue pattern and temperature value during transformation for big undercooling (The corrected images indicate that each top image has been subtracted from the image taken at t-0.2 seconds) - Steel C, Cooling rate: 30ºC/min.

The second mode of δ to γ transformation is depicted in Figure 6, where the solidification behavior is similar to the previous case, but the δ to γ transformation differs significantly. In this mode, the transformation is delayed to a much lower temperature, occurring 78.6°C below the equilibrium calculation, and abruptly, in a very short period (less than 0.2 seconds), the entire δ phase transformed into the γ phase, as shown in the images and Laue pattern in Figure 6. Due to the low frame rate of our experimental setup (5 fps), the δ/γ interface velocity could not be measured in this mode. However, the temperature profile in Figure 7 shows a noticeable temperature peak of 7.1°C, resulting from the rapid release of latent heat. As presented in Table 4, the $t_{0.5}$ time is 0.096 seconds in this case, approximately ten times shorter than in the previous case, indicating a much faster transformation process.

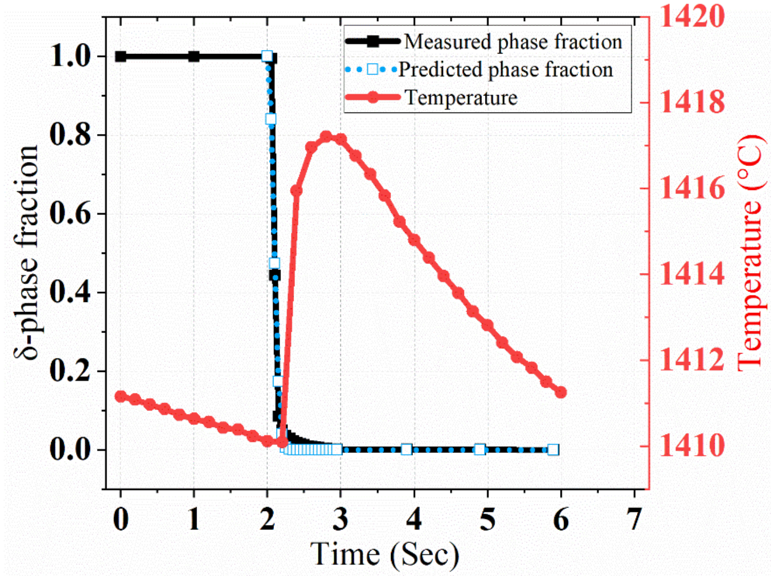

Fig. 7. The temperature profile and phase fraction of the delta phase (measured and predicted) in big undercooling case study- Steel C, Cooling rate: 30°C/min.

In both cases presented above, multiple spot patterns from the gamma phase were detected (in Figure 4 and Figure 6). These multiple diffractions from a single gamma phase indicate that the transformation creates polycrystalline, randomly oriented gamma grains rather than textured ones. The gamma grains originate from multiple, irrational nucleation events which are characteristic of typical massive transformation, as described by Aaronson [27]. Comparing the case between small and high undercooling in Table 3 and 4 respectively, we can deduce that in the Avrami type equation fitting the higher value of n (n=2.1) leads to extensive nucleation and growth activity, while the lower value of n (n=0.85) does limited nucleation, possibly with rapid exhaustion of nucleation driving force. These results align with previous studies by Yasuda et al., [12] which demonstrated that massive-like transitions occur with suppressed nucleation of the gamma phase, followed by an abrupt solid-state delta-to-gamma transition. Yasuda et al., [28] [29] presented sophisticated experimental and analytical results confirming the existence of multiple gamma grains resulting from the delta-to-gamma transition under high undercooling conditions. This evidence supports the conclusion that the degree of undercooling significantly influences the nucleation behavior and resulting microstructure in the gamma phase transformation.

3.3. Experimental results for onset temperature of δ to γ transformation and interfacial velocity

Numerous experiments were conducted to investigate the δ to γ transformation in four peritectic steel grades. The results are presented in Figure 8, where the onset temperature of the transformation is indicated for each grade. The green color signifies that the transformation occurred in the slow mode, as described in the previous section. Generally, in this study, a transformation is classified as slow mode when the duration of the transformation is more than 1 second and the δ/γ interface velocity does not exceed 5 mm/sec.

As the results indicate, both slow and fast transformation modes were observed in all four grades. However, significant differences exist among these steel grades. As presented in Table 5, Steel A exhibits the maximum temperature difference between the liquidus temperature and the minimum δ to γ transformation onset temperature, while Steel D shows the lowest temperature difference. The impact of this temperature variation on solid-shell unevenness will be discussed in the subsequent section

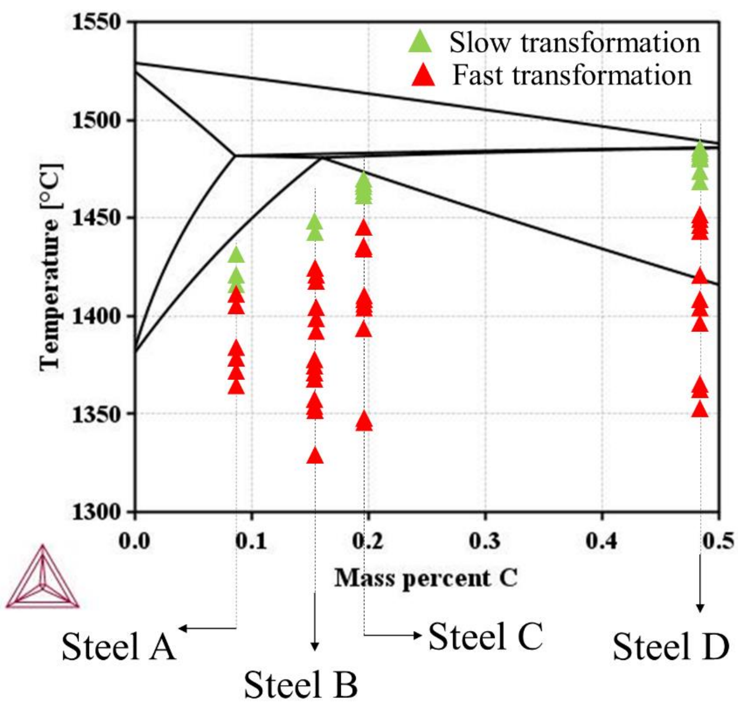

Fig. 8. The measurement of initiation temperature for delta to gamma transformation in four peritectic steel grades

Table 5. Temperature difference between the liquidus and the δ to γ transformation temperature

Steel Code	Minimum $T_l - T_{(\delta \rightarrow \gamma)\ ini}$ (°C)
Steel A	88
Steel B	66.6
Steel C	46.7
Steel D	7.8

T_l= Liquidus temperature

$T_{(\delta \rightarrow \gamma) ini}$= Temperature when γ phase nucleate

The δ/γ interfacial velocity in all four steels shows a dependence on undercooling , as illustrated in Figure 9, ranging from 0.03 mm/sec to 13 mm/sec in measurable cases, with several cases exceeding 16 mm/sec. it should be noted that due to the low frame rate of our experimental setup (5 fps), it was not possible to measure the δ/γ interface velocity accurately when it was faster than 16 mm/sec. The interface velocities observed in Fe-C alloys align with the values quantified for Fe-Cr-Ni alloys studied by T. Nishimura et al [30]. Nishimura's findings indicate that Ni content strongly influences transformation rates, with the 8% Ni alloy displaying much slower interfacial velocities compared to the 11% Ni alloy. This difference is attributed to the partitioning effect, where the smaller quantity of Ni atoms in the 8% Ni alloy facilitates easier partitioning, leading to a delta/gamma transition at the temperature above T0 curve. In the case of the 11% Ni alloy, the delta/gamma transition occurs below the T0 temperature, and the interface migration is driven primarily by massive-like transformation. In Fe-C alloys, at high undercooling levels, the delta/gamma transition occurs significantly below the T0 temperature, and the interface velocity is driven by massive transformation, resulting in a very high speed.

In contrast, the present study on Fe-C alloys shows that the transition rate varies from slow to fast depending on the alloy. Unlike the substitutional Ni atoms, the smaller, interstitial carbon atoms have a fast diffusion rate. The effect of carbon partitioning on the transformation kinetics change would be limited under this fast diffusivity. Instead, carbon influences the minimum undercooling required for the delta/gamma transition and plays a role in gamma phase nucleation, as it will be discussed in Section 4.1. Griesser [31] has confirmed the influence of carbon atom partitioning, showing that it plays a significant role in forming a diffusion field, which inhibits gamma phase nucleation. Another notable difference between this study and the Fe-Cr-Ni cases is the presence of a clear transition between low velocity (less than 5 mm/sec) and high velocity (more than 16 mm/sec) in all the steel grades examined. For each steel, there is a critical amount of undercooling beyond which the interface velocity remains high. However, such a transition was not observed in the Fe-Cr-Ni systems. Furthermore, another study [14] on Fe-0.3C-0.6Mn-0.3Si alloy reported interface velocities based on undercooling. However, all the reported cases showed interface velocities higher than 25 mm/sec, and no data for slower velocities (below 5 mm/sec) were available, making it unclear whether a similar transition exists in this alloy and at what amount undercooling this transition happened.

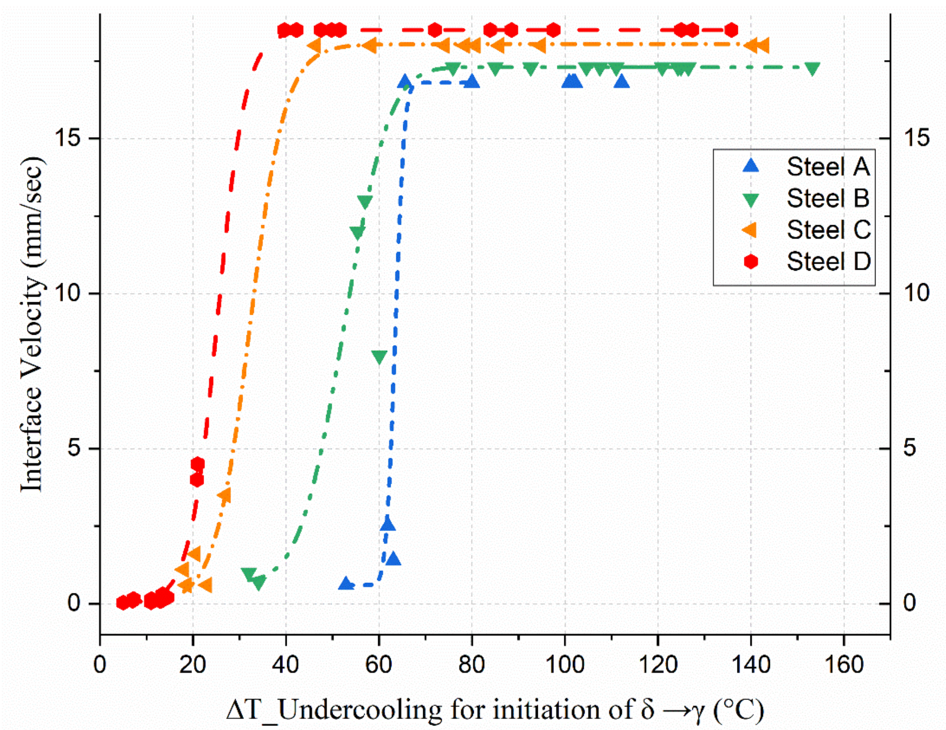

Fig. 9 Variation of interface velocity with the amount of undercooling when delta to gamma transformation occurs.

Another significant finding from these experiments is illustrated in Figure 10. This figure depicts the relationship between cooling rate and the temperature of δ to γ transformation for Steel A. As shown, there is no correlation between the cooling rate and the onset temperature of transformation or the mode of transformation. Table 6 presents the results of 10 selected experiments for each steel grade, conducted at varying cooling rates. It is evident that the cooling rate does not influence the nucleation temperature of the γ phase. This aligns with the findings of Nishimura et al. [30] , who investigated Fe-Cr-Ni alloys with cooling rates between 10 and 100ºC/min and couldn't confirm the influence of the cooling rate. The observed variation in transformation temperatures can be attributed to the presence of heterogeneous nucleation sites within the material. Surface effects and microstructural irregularities can significantly affect nucleation behavior in real systems, leading to slight differences in activation temperatures for different sites, even under identical cooling conditions. Therefore, the onset temperature for the δ to γ transformation is determined by how easily the γ phase can nucleate and is independent of the cooling rate. Additionally, the mode of transformation (slow or fast) is solely dependent on the amount of undercooling rather than the cooling rate. A bigger degree of undercooling results in a transition to a fast mode of transformation.

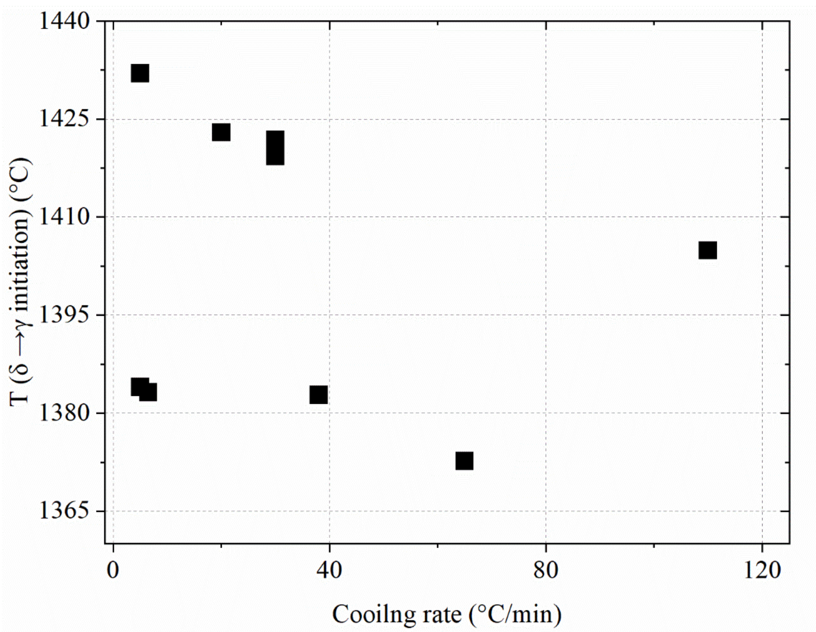

Fig. 10. Cooling rate and the temperature of initiation of δ to γ transformation in steel grade A

Table 6. The Cooling rate, equilibrium temperature of initiation of δ to γ: $T^{E}_{\delta \text{ to } \gamma}$,and measured temperature of initiation of δ to γ: $T^{m}_{\delta \text{ to } \gamma}$ for selected cases of four steel grades

Steel A $T^{E}_{\delta \text{ to } \gamma}$: **1484.9 ºC**		**Steel B** $T^{E}_{\delta \text{ to } \gamma}$: **1481 ºC**		**Steel C** $T^{E}_{\delta \text{ to } \gamma}$: **1488 ºC**		**Steel D** $T^{E}_{\delta \text{ to } \gamma}$: **1490ºC**	
C.R (ºC/min)	$T^{m}_{\delta \text{ to } \gamma}$ (ºC)	C.R (ºC/min)	$T^{m}_{\delta \text{ to } \gamma}$ (ºC)	C.R (ºC/min)	$T^{m}_{\delta \text{ to } \gamma}$ (ºC)	C.R (ºC/min)	$T^{m}_{\delta \text{ to } \gamma}$ (ºC)
5	1432	20	1356.7	5	1461.6	5	1482.8
5	1384	30	1405.1	6.5	1393.7	5	1479
6.5	1383.2	30	1370	30	1410.1	5	1438.4
20	1423	110	1449	30	1402.7	30	1483
30	1421.8	110	1396	40	1442.2	30	1469
30	1419.3	110	1388.4	40	1345.7	30	1354.2
40	1382.8	110	1376.4	110	1470.6	50	1478.8
65	1372.7	290	1425.6	110	1407.8	50	1447.7
110	1404.9	500	1424	270	1468	55	1418
---	----	500	1373.5	460	1430.4	110	1450.3

4. Discussion

4.1. Influence of carbon content on formation of the gamma phase

The investigation into the variation of minimum undercooling required to induce γ phase formation during the cooling of four different steel alloys provides valuable insights into the complex interplay between carbon content, cooling rates, and phase transformation dynamics. In this study, the starting temperature of γ phase formation was meticulously detected using X-ray transmission images coupled with corresponding Laue diffraction spots. The key metric of interest, undercooling, was defined as the temperature difference between the γ phase nucleation onset and the equilibrium peritectic temperature (T_{peri}) (Equilibrium δ to γ onset temperature). This undercooling value indicates the driving force for transforming from the δ phase to the γ phase during cooling. The experimental setup allowed for precise measurement of undercooling across various cooling rates, thereby enabling the determination of minimum and maximum undercooling values for each steel alloy system. We could infer the carbon concentration at the metastable interface between the δ and the remaining liquid phases by examining the temperature at which γ phase nucleation begins. The meta-stable state is likely maintained by increased γ phase free energy due to the nucleation barrier and external energy source. According to the constrained nucleation theory [8], the role of carbon content is crucial here, as it directly influences the nucleation and growth of the γ phase. The schematic free energy diagram for the meta-stable state of the δ, liquid and γ phases is presented in Figure 11-a.

The X-ray topography analysis further verified whether the peritectic reaction, indicative of γ phase formation at the liquid/ δ phase boundary, occurred under the required undercooling below T_{peri}. In steel A and B, the carbon content is in the hypo-peritectic region, and the peritectic reaction did not appear, and the γ phase formation requires significant undercooling. However, steel C and D displayed the peritectic reaction under T_{peri}, and even in steel D, we were able to observe the γ phase growth followed by the mobile interface between δ and liquid.

Since all four steel alloys show supercooling, we can consider the metastable state shown in Figure 12 and extend the solidus line below the T_{peri} temperature through the δ and the liquid phase. Utilizing the TCFE13 thermodynamic database, we accurately mapped the δ-solidus line for each alloy, providing a basis for analyzing the carbon concentration and its impact on phase transformation. As presented in Table 7, among the four steel alloys studied—A, B, C, and D—distinct differences in carbon concentration were observed, which played a significant role in the observed undercooling behaviour. Alloy A, characterized by the lowest initial carbon concentration in the primary δ phase, exhibited the most remarkable difference in carbon content between the initial solid state and the undercooled state. This significant disparity resulted in the steepest concentration gradient among the solid δ, which in turn significantly retarded the nucleation of the γ phase at the interface between δ and liquid. The steep concentration gradient creates a substantial carbon diffusion field, which poses a challenge to the stabilization of the γ nuclei, as this phase must accommodate more carbon than the δ phase. The nucleation of the γ phase is further hindered by adiabatic conditions, primarily influenced by the cooling rate. The results revealed that Steel A, with the lowest carbon concentration in the primary δ phase, exhibited the highest carbon supersaturation at the δ/liquid interface. This high level of supersaturation creates a strong carbon diffusion potential into the δ phase, which acts as a destabilizing factor for the γ phase. The γ phase, which must grow into the δ phase, is hindered by this carbon-rich environment, delaying its formation until a lower temperature range. Once nucleation does occur, the process is driven by a significant undercooling, resulting in a rapid and like a massive phase transition. In the massive transformation, we can deduce the driving force for the growing interface by using the undercooling from the T_0 point, defined by equating free energies between two phases. The concept of T_0 temperature is illustrated in Figure 11-(b) for the delta and gamma phases. The observed decrease in interfacial velocity from Material A to Material D is consistent with the decrease in T_0 values observed for the same materials. As the carbon content increases, the minimum undercooling gradually decreases, which indicates that the generation of the γ phase is becoming increasingly more accessible. Therefore, the carbon concentration of the ultimate δ phase, determined from the extended solid phase in Figure 12, gradually decreases. The decreased carbon content in the undercooled δ phase slows down the carbon migration and increases the stability of the γ nuclei. This trend is most pronounced in steel D. It almost follows the equilibrium phase transition and around the T_{peri} temperature the γ phase appears. Therefore, it can be seen that steel D does not exhibit massive transformation driven by the undercooling from the T_0 temperature. However, the growth of the γ phase occurs by carbon diffusion and redistribution at a given temperature. Consequently, the growth rate is much slower than that of steel A, which is transformed rapidly, and in a massive-like manner when the same undercooling is applied.

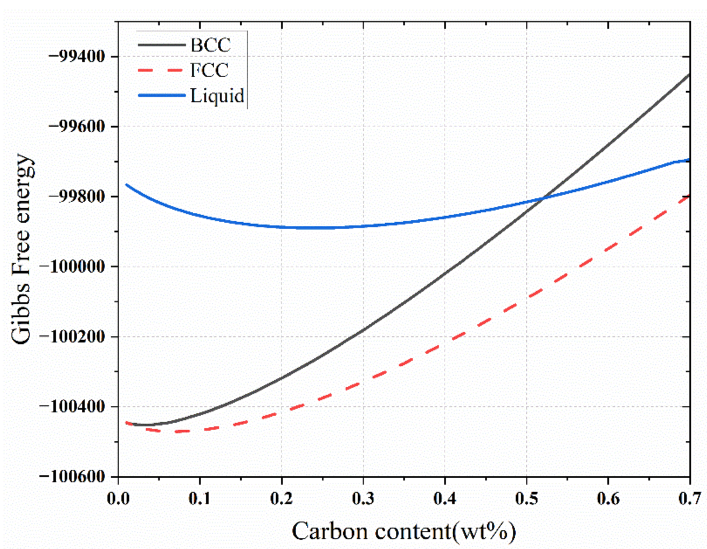

Fig 11 – (a)

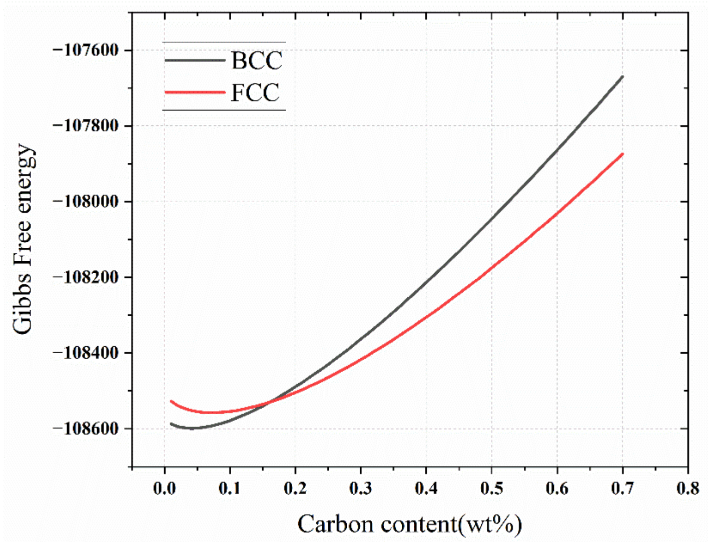

Fig 11 – (b)

Fig.11. Free energy diagram of meta stable condition of steel A at temperature of 1431C (a), and the T0 temperature (1509 ºC) determination between delta and gamma with the carbon content 0.162wt%, at the minimum undercooling temperature (1431 ºC)

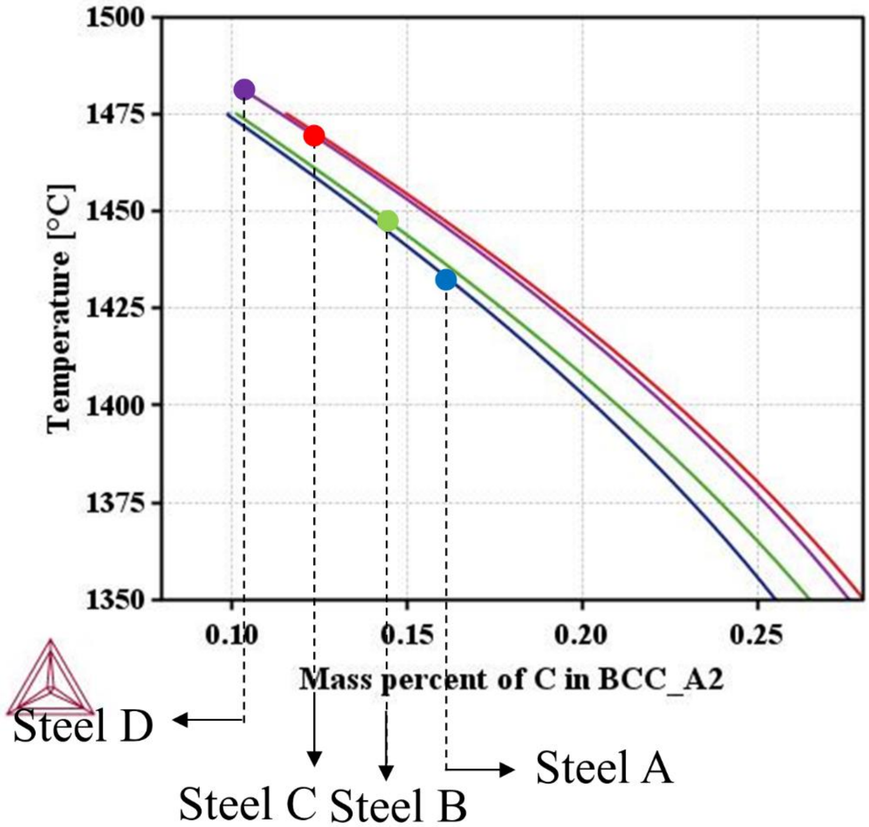

Fig. 12. The extended solidus line of the steel alloys at the meta stable equilibrium condition**.**

Table 7. The carbon contents, undercooling and T_0 temperatures of investigated steel alloys.

Alloys	**Steel A**	**Steel B**	**Steel C**	**Steel D**
Initial [C] of primary delta	0.019	0.011	0.026	0.073
Min. undercooling Temp. (°C)	1431	1449	1470.6	1485
[C] at min undercooling Temp.	0.162	0.142	0.123	0.103
T_0 at min undercooling Temp. (°C)	1509	1493	1487.5	1474

4.2. The correlation of interface velocity to slab quality in continuous casting

The delta/gamma interfacial velocity in all four steels demonstrates a dependence on undercooling, as illustrated in Figure 9. The migration speed of the delta/gamma interface exhibits the most dramatic variation in Steel A among the steel grades studied. As previously discussed, Steel A requires a considerably higher degree of undercooling than other steel grades at the point where the gamma phase begins to nucleate and grow, and variations in undercooling temperature on the order of 2 to 3 degrees cause significant disparities in the interfacial velocity as presented in Table 8 and Figure 9. This pronounced change in the interfacial migration velocity is particularly problematic when considering the solid shell that forms on the mould surface during the continuous casting process. In continuous casting, the solid shell plays a critical role in maintaining the structural integrity of the slab as it moves through the mould. However, at the mould-side surface, the solid shell often exhibits variations in thickness from the meniscus surface to the bottom of the mould. The thickness variations result in corresponding fluctuations in temperature and undercooling between the thinner and thicker regions of the shell, illustrated in Figure 13.

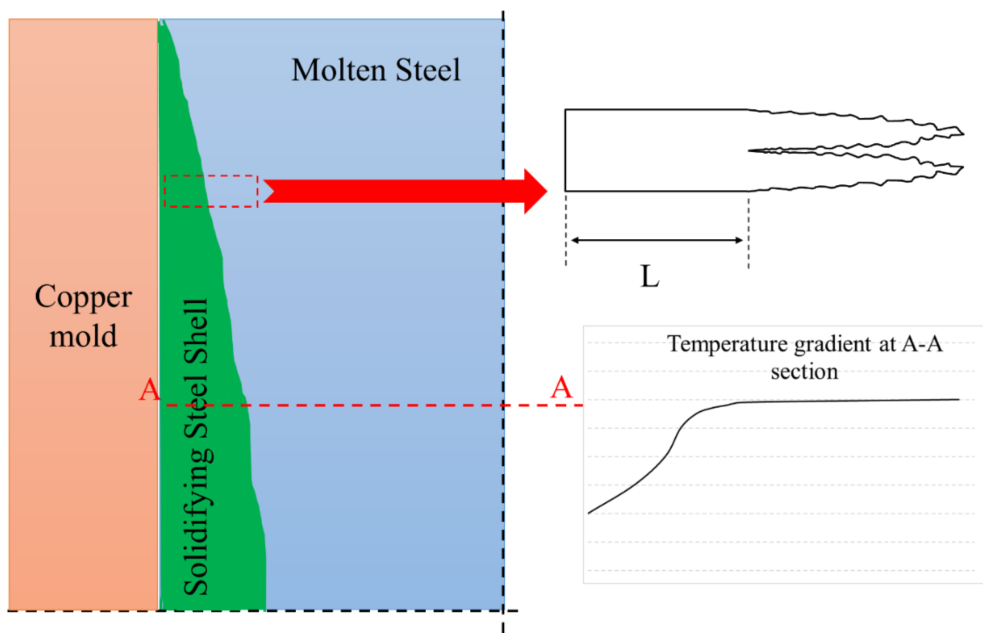

Fig. 13 Illustrated situation at the mould-side wall during solidification. The temperature gradient from molten steel to the solid shell gives rise to variations of undercooling and subsequent abrupt change in interface velocity of delta to gamma transition.

As demonstrated in Table 8, the undercooling variations manifest in a sharp difference because of the rapid change of phase transformation rate within a narrow area in Steel A. It disrupts the uniformity of the solidification process and significantly accelerates the accumulation of stress within the solidifying material. The stress accumulation is due to the volume expansion accompanying the phase transformation. In areas where the phase transition occurs more rapidly, the localized expansion can create internal stresses that lead to the deformation of the solid shell. This deformation is particularly concerning because it can result in surface defects, such as unevenness and cracks, which compromise the quality of the final product. The correlation of abrupt change in transformation rate and the slab quality is consistent with historical data and simulations that model the behaviour of steel under actual operating conditions in continuous casting [32] [33] [34] [35]. The measured depth profiles from our previous study [35] are plotted alongside the average required undercooling for fast transformation for these four steels in Figure 14. For both Steels A and B, the profile depth by which the surface quality of the slab—such as the uniformity of the solid shell—can be evaluated is significantly greater than other steel grades. The deeper profile suggests that the effects of non-uniform solidification extend further into the slab, making it more difficult to control and correct surface defects during subsequent processing stages. The interfacial velocity accelerates rapidly as the undercooling temperature increases, leading to a more abrupt and uneven phase transition. This rapid phase change not only affects the surface geometry of the slab, resulting in issues such as surface roughness and unevenness, but it also increases the risk of more severe defects. One of the most concerning potential defects is the formation of surface cracks, which can occur due to the strain accumulation associated with localized changes in the delta/gamma interfacial behaviour. The increased tendency of surface cracks in Steel A is primarily driven by the strain that builds up during the rapid phase transition. If the strain is not evenly distributed, it can initiate cracks, particularly in areas where phase transition occurs more quickly. The localized nature of these changes in interfacial velocity means that some areas of the slab are more susceptible to cracking than others, making it difficult to predict and control the formation of defects.

In summary, the transition behaviour of Steel A's delta/gamma interfacial velocity highlights several critical challenges associated with its use in continuous casting. The sensitivity to undercooling and the resulting sharp variations in interfacial velocity contribute to significant stress accumulation and an increased risk of surface defects. Addressing these issues requires careful control of the casting process, including precise management of cooling rates and close monitoring of the solidification front, to minimize the impact of these factors on the final product quality

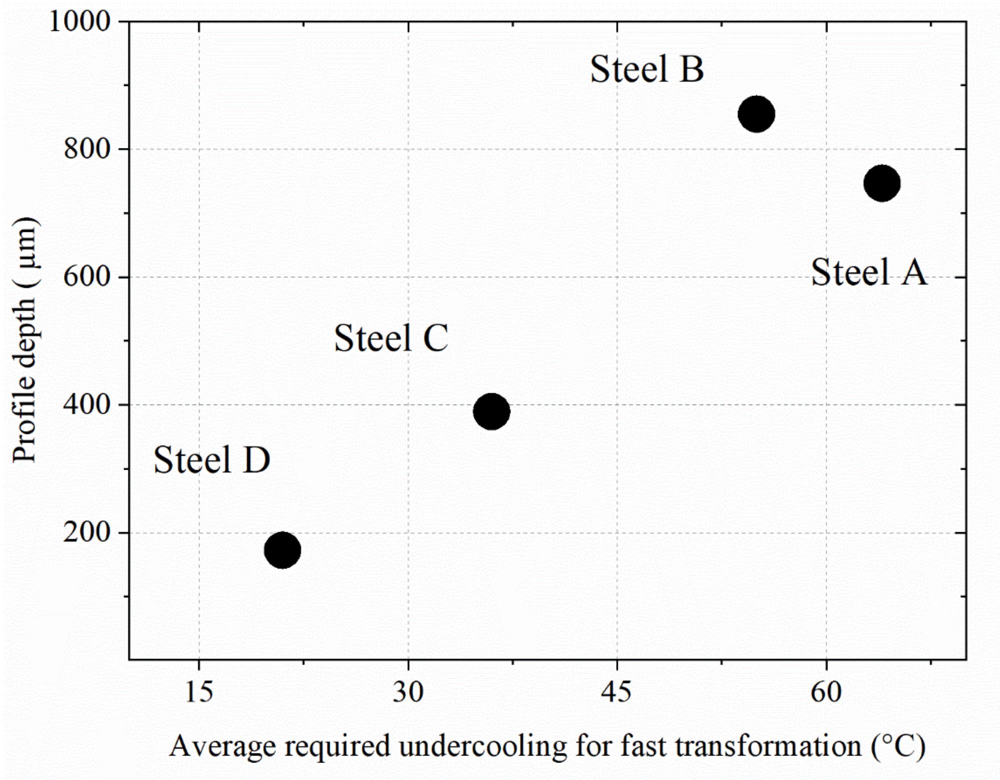

Fig. 14 Correlation of profile depth at slab surface to the required undercooling [35]

Table 8 Comparison of profile depth, undercooling and transition properties for steel alloys

grade	**Profile Depth (µm)**	**Min. undercooling required for onset of transition (°C)**	**ΔT gap between slow and fast transition (°C)**
Steel A	746.8	52	3
Steel B	855.1	33	32
Steel C	389.5	18	20
Steel D	172.6	5	20

5. Conclusion

Our investigation examined the phase transformation behaviour of peritectic steel alloys with varying carbon content using in-situ X-ray transmission images with Laue diffraction. The transmission image and diffraction signal, combined with precise temperature control, allowed us to observe the real-time solidification process, including the liquid-to-solid phase transformation and the solid-state delta (δ) to gamma (γ) phase transition. The results indicate a clear relationship between carbon content and the behaviour of the peritectic reaction. Specifically, when the nominal carbon content is low, the peritectic reaction is suppressed, requiring significant undercooling for the gamma phase to form. Conversely, higher carbon content facilitates gamma-phase nucleation even with minimal undercooling. The difference in transformation behaviour is due to the suppressed gamma phase nucleation at low carbon levels, which leads to rapid, massive transformation at lower temperatures.

In contrast, higher carbon content enables gamma nucleation at more minor undercooling levels but with a slower interface velocity. The dependence of the minimum undercooling on carbon content supports the constrained nucleation theory, as the required undercooling for γ phase formation increases with the carbon content difference between the primary and supersaturated δ phase, where significant carbon diffusion potential exists. Additionally, our analysis revealed that steel with a carbon content near the lower limit of the peritectic range shows pronounced sensitivity to undercooling. Increasing carbon content results in compromising the sensitivity to undercooling. Our experimental work offers a valuable method for mitigating slab defects in peritectic steels, particularly in alloys with approximately 0.1 wt% carbon, where the addition of element Si can reduce the carbon migration potential and enhance the nucleation of the gamma phase below the peritectic temperature.

Acknowledgments

This research is supported by POSCO steelmaking company in South Korea (Project number: 4.0026102.01).

References

1. De Cooman, B., *Structure–properties relationship in TRIP steels containing carbide-free bainite.* Current Opinion in Solid State and Materials Science, 2004. **8**(3-4): p. 285-303.
2. Jacques, P., *Phase transformations in transformation induced plasticity (TRIP)-assisted multiphase steels*, in *Phase transformations in steels*. 2012, Elsevier. p. 213-246.
3. Tamura, I., H. Sekine, and T. Tanaka, *Thermomechanical processing of high-strength low-alloy steels*. 2013: Butterworth-Heinemann.
4. Kerr, H.W., J. Cisse, and G. Bolling, *On equilibrium and non-equilibrium peritectic transformations.* Acta Metallurgica, 1974. **22**(6): p. 677-686.
5. Shibata, H., et al., *Kinetics of peritectic reaction and transformation in Fe-C alloys.* Metallurgical and Materials Transactions B, 2000. **31**: p. 981-991.
6. Fredriksson, H. and T. Nylen, *Mechanism of peritectic reactions and transformations.* Metal Science, 1982. **16**(6): p. 283-294.
7. Chen, Y., et al., *Nonequilibrium effects of primary solidification on peritectic reaction and transformation in undercooled peritectic Fe–Ni alloy.* Journal of Materials Research, 2010. **25**(6): p. 1025-1029.
8. Griesser, S., et al., *Diffusional constrained crystal nucleation during peritectic phase transitions.* Acta materialia, 2014. **67**: p. 335-341.
9. Nishimura, T., et al., *Time-resolved and In-situ Observation of δ–γ Transformation during Unidirectional Solidification in Fe–C Alloys.* isij international, 2020. **60**(5): p. 930-938.
10. Phelan, D., M. Reid, and R. Dippenaar, *Kinetics of the peritectic reaction in an Fe–C alloy.* Materials Science and Engineering: A, 2008. **477**(1-2): p. 226-232.
11. Umeda, T., T. Okane, and W. Kurz, *Phase selection during solidification of peritectic alloys.* Acta Materialia, 1996. **44**(10): p. 4209-4216.
12. Yasuda, H., et al. *Massive transformation from δ phase to γ phase in Fe–C alloys and strain induced in solidifying shell*. in *IOP conference series: materials science and engineering*. 2012. IOP Publishing.
13. Ueshima, Y., et al., *Analysis of solute distribution in dendrites of carbon steel with δ/γ transformation during solidification.* Metallurgical Transactions B, 1986. **17**: p. 845-859.
14. Nishimura, T., et al. *Kinetics of the δ/γ interface in the massive-like transformation in Fe-0.3 C-0.6 Mn-0.3 Si alloys*. in *IOP Conference Series: Materials Science and Engineering*. 2015. IOP Publishing.
15. Sarkar, R., et al., *Effects of alloying elements on the ferrite potential of peritectic and ultra-low carbon steels.* ISIJ international, 2015. **55**(4): p. 781-790.
16. Wolf, M., *Initial solidification and strand surface quality of peritectic steels*. 1997: Iron & Steel Society.
17. Xia, G., et al., *Investigation of mould thermal behaviour by means of mould instrumentation.* Ironmaking & steelmaking, 2004. **31**(5): p. 364-370.
18. Boussinot, G., et al., *Isothermal solidification in peritectic systems.* Acta materialia, 2014. **75**: p. 212-218.
19. Lopez, H., *Analysis of solute segregation effects on the peritectic transformation.* Acta metallurgica et materialia, 1991. **39**(7): p. 1543-1548.
20. Ha, H. and J. Hunt, *A numerical and experimental study of the rate of transformation in three directionally grown peritectic systems.* Metallurgical and Materials Transactions A, 2000. **31**: p. 29-34.

21. Das, A., I. Manna, and S. Pabi, *A numerical model of peritectic transformation.* Acta materialia, 1999. **47**(4): p. 1379-1388.
22. Liu, N., et al., *Peritectic solidification of undercooled Fe–Co alloys.* Journal of alloys and compounds, 2008. **465**(1-2): p. 391-395.
23. Zargar, T., et al., *In-situ observation on the δ to γ transformation behavior of carbon steels.* Materialia, 2023. **32**: p. 101960.
24. Zamanian, A., et al., *Analysis of high temperature phase transformation behavior of ultra-low-carbon steel using X-ray topography, diffraction, and synchronized temperature measurement.* Materialia, 2024: p. 102137.
25. Azizi, G., B.G. Thomas, and M. Asle Zaeem, *Review of peritectic solidification mechanisms and effects in steel casting.* Metallurgical and Materials Transactions B, 2020. **51**: p. 1875-1903.
26. Normanton, A., et al., *Improving surface quality of continuously cast semis by an understanding of shell development and growth.* 2005.
27. Aaronson, H.I., *Mechanisms of the massive transformation.* Metallurgical and materials transactions A, 2002. **33**: p. 2285-2297.
28. Yasuda, H., et al., *Dendrite fragmentation induced by massive-like δ–γ transformation in Fe–C alloys.* Nature communications, 2019. **10**(1): p. 3183.
29. Yasuda, H., et al., *Transformation from ferrite to austenite during/after solidification in peritectic steel systems: an X-ray imaging study.* isij international, 2020. **60**(12): p. 2755-2764.
30. Nishimura, T., et al., *Selection of the massive-like δ-γ transformation due to nucleation of metastable δ phase in Fe-18 mass% Cr-Ni alloys with Ni contents of 8, 11, 14 and 20 mass%.* isij international, 2019. **59**(3): p. 459-465.
31. Griesser, S., C. Bernhard, and R. Dippenaar, *Effect of nucleation undercooling on the kinetics and mechanism of the peritectic phase transition in steel.* Acta materialia, 2014. **81**: p. 111-120.
32. Jiang, Z.-k., et al., *Abnormal mold level fluctuation during slab casting of peritectic steels.* Journal of Iron and Steel Research International, 2020. **27**: p. 160-168.
33. Li, Y., et al., *Control of mould level fluctuation through the modification of steel composition.* International Journal of Minerals, Metallurgy, and Materials, 2013. **20**: p. 138-145.
34. Furumai, K., et al., *Influence of mould level instability on the unevenness of solidified shell deformations during continuous casting.* Ironmaking & Steelmaking, 2023. **50**(7): p. 818-827.
35. Kwon, S.-H., et al., *Prediction model for degree of solid-shell unevenness during initial solidification in the mold.* ISIJ International, 2021. **61**(10): p. 2534-2539.